



## Comparison of ion exchange process configurations for arsenic removal from natural waters

Markku Laatikainen\*, Mika Sillanpää, Tuomo Sainio

LUT School of Engineering Science, Lappeenranta University of Technology, Skinnarilankatu 34, FI-53850 Lappeenranta, Finland, emails: [markku.laatikainen@lut.fi](mailto:markku.laatikainen@lut.fi) (M. Laatikainen), [mika.sillanpaa@lut.fi](mailto:mika.sillanpaa@lut.fi) (M. Sillanpää), [tuomo.sainio@lut.fi](mailto:tuomo.sainio@lut.fi) (T. Sainio)

Received 16 March 2015; Accepted 3 June 2015

### ABSTRACT

Influence of process configuration on ion exchange of As(V) was studied using numerical simulations. A new explicit competitive ion exchange model was introduced to facilitate fast computation. Model parameters were determined using published data on arsenic removal from contaminated waters by hydrous ferric oxide (HFO) hybrid materials and strong anion exchangers (SBA). Performance of batch and continuous processes was assessed in terms of productivity and resin utilization. It was shown that the HFO resin with very high As(V) selectivity is best utilized in batch operation and counter-current simulated moving bed (SMB) configuration does not give any advantage. The SBA resin has low selectivity for As(V) anions and counter-current operation was found to be essential. A steady state SMB system with continuous removal of the concentrated As(V) fraction was proposed. It was also shown that productivity of both systems can be substantially increased using shallow beds and short loading cycles.

*Keywords:* Arsenic removal; Ion exchange; Modeling; Batch operation; Simulated moving bed

### 1. Introduction

Arsenic removal from surface and ground waters is a globally important issue. In many areas, water contamination by geothermal processes and mining activities results in high-risk arsenic levels in water supplies. Toxicity of arsenic is due to its tendency to cause skin, liver, lung, and kidney cancer. Maximum concentration in drinking water recommended by EU and WHO is 10 µg/L, while order of magnitude higher values are often found in water resources [1] and strong local seasonal variation is observed in monsoon regions [2].

Depending on the redox conditions, arsenic is present as As(III) and/or As(V) oxoanions. The former is predominant in ground waters and the latter in surface waters [3]. As(III) species are known to be more toxic than arsenates but because of easy reduction of the latter *in vivo*, removal of As(V) is equally important [4]. In neutral solutions, trivalent arsenic exists as undissociated arsenous acid,  $\text{H}_3\text{AsO}_3$ , and is more difficult to remove than the dissociated arsenate anions,  $\text{H}_2\text{AsO}_4^-$  and  $\text{AsO}_4^{2-}$ . Pre-oxidation to As(V) is thus often used. Conventionally arsenic is removed by precipitation with ferric salts, by adsorption using granular ferric oxide or alumina and by anion exchange. Advantages and disadvantages of various arsenic removal methods have been reviewed by

\*Corresponding author.

Kartinen and Martin [5] and sorption processes have been compared by Mohan and Pittman [6] and Dambies [7].

Ion exchange of the As(V) species with strong anion exchangers (SBA) has been studied by several investigators [8,9]. Major drawback of this method is the unfavorable selectivity order; the resin is more selective for naturally existing anions such as sulfate and nitrate, and the capacity for arsenate anions is therefore relatively low. Short loading cycles must therefore be used and large amounts of As-contaminated brine are produced in the regeneration step. Therefore, more selective exchangers have been developed [4,10,11] and hybrid materials containing hydrous ferric oxide (HFO) nanoparticles in SBA are also commercially available [12,13]. High selectivity for As(V) anions has been explained by formation of inner sphere complexes with the HFO nanoparticles embedded in the polymer matrix [10]. As a result, the loading capacity for arsenic species is markedly increased. A process combining ion exchange with SBA and with As-selective sorbent has been proposed for waters containing high concentrations of silicates [13].

While a lot of effort has been directed to development of separation materials, investigation of process configurations has not received sufficient attention. In most cases, ion exchange of arsenic has been studied using single-column systems, where loading and elution/regeneration steps are carried out consecutively in a batchwise manner. Advantages of this configuration are simplicity and ease of operation. More efficient use of the resin can be achieved by optimizing the length of the resin bed and/or using simulated moving bed (SMB) systems in counter-current or cross-current configuration. Short bed technology, where the bed length is of the same order as the length of the exchange zone, is well established in various applications of ion exchange. Short loading cycles are used to ensure more efficient use of the resin capacity.

Counter-current concept has been applied by Kim and Benjamin [14] in arsenic ion exchange using a sulfate selective SBA. Their system consists of a 2-column loading zone and a separate regeneration zone with periodical switch of the inlet and outlet positions. Because of the selectivity order, sulfate is more strongly bound and it is removed from the resin during the regeneration step. Arsenic accumulates in the downstream column of the loading zone and is not continuously removed. In other words, the system is operated at non-steady conditions until As(V) breakthrough from the downstream column. A similar process has been studied also by Chiavola et al. [9].

Simple lead-lag configuration used in As(V) removal [15] may also be considered as a counter-current operation. Two identical beds are used and the feed is in the lead column and product water is taken out from the downstream or lag column. After exhaustion, the lead column is replaced by the lag column and the regenerated bed is placed as the lag column.

The objective of this study is to analyze performance of various process configurations in removal of arsenic from ground and surface waters with ion exchange. Two cases are studied; HFO-based hybrid material having high selectivity for the arsenate ions and conventional anion exchanger with low selectivity for As(V) species. The former case thus represents a system, where the target impurity is most strongly sorbed and extremely long loading times can be used. Moreover, specific treatment is needed in the regeneration step to destroy the stable arsenate complex formed on the HFO surface. The second case is an example of reversible ion exchange. The two systems are simulated using equilibrium and mass transport models that allow fast computation. Ion exchange equilibrium is described using an equation derived from the non-ideal competitive adsorption (NICA) model and an approximate solution of the Nernst-Planck equation is used for ion diffusion. Arsenic removal in fixed beds arranged in different batch or continuous configurations is simulated and the results are discussed in terms of productivity and As(V) loading efficiency.

## 2. Computational methods

### 2.1. Data

No experimental data were generated in this study, but all values were taken from literature. Only breakthrough curves were available and independent determination of equilibrium or kinetic parameters was not possible.

The data measured by Cumbal and SenGupta [10] were used to estimate the model parameters for As(V) removal with hybrid HFO material. This resin is composed of HFO nanoparticles dispersed within a gel-type anion exchanger composed of a poly(styrene-co-divinylbenzene) matrix and containing quaternary ammonium groups. Cumbal and SenGupta [10] have discussed the role of the fixed positive charges of the matrix in terms of the Donnan equilibrium. In order to simplify the calculation procedure, the influence of the matrix charge is not explicitly considered in the following treatment and only ion exchange at the HFO particles is taken into account. Active sites on HFO are the hydroxyl groups, which can protonate or

deprotonate depending on solution pH. At neutral conditions, part of the groups exists in the form (HFO)–OH<sub>2</sub><sup>+</sup> thus allowing uptake of the anionic species. In the following calculations, the hybrid structure is approximated as a pseudo-homogeneous gel, where the (HFO)–OH<sub>2</sub><sup>+</sup> sites are evenly distributed and equally accessible to the ions. Moreover, amount of sites is assumed to be constant and a value of 0.25 equiv/kg was estimated on the basis of the position of the experimental breakthrough curve. Composition of the feed solution and the operating conditions are listed in Table 1. Solution pH was found to remain practically constant at 7.2–7.3 for the loading step. At these conditions, As(V) is present as nearly equimolar mixture of H<sub>2</sub>AsO<sub>4</sub><sup>−</sup> and HAsO<sub>4</sub><sup>2−</sup> anions (pK<sub>a,2</sub> = 6.98) [10]. Moreover, the ionic strength was constant because the resin was rapidly saturated by the major anions. Therefore, no speciation scheme was included in the model, but arsenic(V) was treated as a univalent anionic pseudo-component H<sub>2</sub>AsO<sub>4</sub><sup>−</sup>. In the regeneration step with NaOH [10], AsO<sub>4</sub><sup>3−</sup> is the main arsenate component, but this stage is not considered in calculations. In a similar way, the dissociation constants of carbonic acid are pK<sub>a,1</sub> = 6.4 and pK<sub>a,2</sub> = 10.3 suggesting that both undissociated form and the bicarbonate anion exist at neutral conditions. Sorption of the neutral acid was, however, neglected in calculations.

Removal of As(V) with SBA was simulated using the breakthrough data reported by Kim and Benjamin [14]. Standard gel-type resin with a poly(styrene-co-divinylbenzene) matrix and with quaternary ammonium groups (type I, Ionac ASB-1, Sybrom Chemicals) was

used in their experiments and according to Tripp and Clifford [16], dry weight capacity is 3.6 equiv/kg. The experimental conditions are given in Table 1. Solution pH was again close to neutral (7.2), but due to separation of the major ions, the ionic strength varied strongly during the run (see Section 3.1).

The bed dimensions and flow rates reported in the original papers were used in calculations and average particle diameter of both resins was taken as 0.5 mm.

## 2.2. Methods

### 2.2.1. Model development

Axial concentration profiles in fixed bed columns considered in this study were calculated using a discrete model, where the continuous resin bed is approximated by  $N$  stirred tanks in series. In this approach, the partial differential mass balance equation is replaced by the ordinary differential equation given in Eq. (1). Here,  $c$  is the solution concentration,  $q$  is adsorbed amount,  $v$  is interstitial flow velocity,  $t$  is time,  $\varepsilon_b$  is bed porosity, and  $\rho_s$  is resin density. Bed porosity was assumed constant and a value  $\varepsilon_b = 0.40$  was used in calculations. The resin density was not known and values  $\rho_s = 0.65$  and  $0.80$  kg/L were used for the SBA and HFO resins, respectively. Here, the density means the solid content in the swollen resin and it was assumed to remain constant for a given resin. The over-bar in Eq. (1) indicates volume-averaged value (see below).  $L_b$  is the length of the bed and  $k$  is the index of the tank (i.e. axial position). At  $k = 1$ , the concentrations are equal to the feed concentrations.

Table 1  
Experimental conditions

	HFO resin [10], $q_{\max} = 0.25$ equiv/kg	SBA resin [14], $q_{\max} = 3.60$ equiv/kg
Feed solution (mg/L (mol/L))		
Sulfate	120 ( $1.25 \times 10^{-3}$ )	125 ( $1.3 \times 10^{-3}$ )
Chloride	100 ( $2.8 \times 10^{-3}$ )	0
Nitrate	0	29 ( $0.47 \times 10^{-3}$ )
Bicarbonate	100 ( $1.6 \times 10^{-3}$ )	0
Arsenic	0.100 ( $1.3 \times 10^{-6}$ )	0.042 ( $0.53 \times 10^{-6}$ )
Conditions		
EBCT <sup>a</sup> (min)	3.9	3.77
SLV <sup>b</sup> (m/h)	0.60	–
Bed volume (mL)	3.7	10
Feed flow rate (mL/min)	0.95	2.65
pH	7.2–7.3	7.2

<sup>a</sup>Empty bed contact time.

<sup>b</sup>Superficial liquid velocity.

$$\frac{dc_{i,k}}{dt} + v \frac{N(c_{i,k} - c_{i,k-1})}{L_b} + \left( \frac{1 - \varepsilon_b}{\varepsilon_b} \right) \rho_s \frac{d\bar{q}_{i,k}}{dt} = 0 \quad (1)$$

$(k = 2 \dots N + 1)$

Axial dispersion is not explicitly accounted for in Eq. (1), but the dispersion coefficient  $D_{ax}$  is approximately related to  $N$  as shown in Eq. (2) [17].

$$D_{ax} \approx \frac{vL_b}{2N} \quad (2)$$

The last term on the left-hand side of Eq. (1) is due to accumulation of the ions in the solid phase. Mass transfer rate of ions is conventionally described using the Nernst-Planck equation. However, computing of the radial concentration profiles is time consuming and, therefore, a simplified treatment proposed by Melis et al. [18] was adopted here. Their approach is based on the linear driving force approximation, where the intraparticle concentration profiles are replaced by average concentrations. Moreover, the electrostatic constraint included in the Nernst-Planck equation is retained also in the simplified version. Consequently, accumulation of ion  $i$  can be expressed as in Eq. (3), where  $D_s$  and  $d_s$  are diffusion coefficient and particle diameter. Over-bar and asterisk refer to the volume-averaged value and value at the solid-liquid interface, respectively.

$$\frac{\partial \bar{q}_i}{\partial t} \approx - \frac{60D_{s,i}}{d_s^2} \left[ (q_i^* - \bar{q}_i) - z_i q_i^* \frac{\sum_j D_{s,j} (q_j^* - \bar{q}_j)}{\sum_j z_j D_{s,j} q_j^*} \right] \quad (3)$$

Because external film diffusion is omitted in the present study,  $q^*$  is obtained from the bulk solution concentrations using suitable phase equilibrium model. Uptake of ions from solution onto HFO and other metal oxides has been conventionally described using various surface complexation models (SCM) [19,20]. A more straightforward approach was used in this study in order to simplify calculations. The iterative solution of SCM was avoided by employing an explicit ion exchange isotherm derived from the NICA model of Kinniburgh et al. [21]. This model was also used for ion exchange in the SBA resin.

The NICA model is a general adsorption isotherm equation relating the adsorbed amount  $q$  to concentrations of all competing species  $c$  (Eq. (4)). Here,  $K$  is affinity constant,  $h$  is a parameter related to adsorption stoichiometry and lateral interactions, and  $p$  is a site heterogeneity parameter. Subscript ref stand for reference component.

$$q_i = q_{max} \frac{h_i}{h_{ref}} \frac{(K_{i,k}c_i)^{h_i} \left[ \sum_j (K_jc_j)^{h_j} \right]^{p-1}}{1 + \left[ \sum_j (K_jc_j)^{h_j} \right]^p} \quad (4)$$

As all adsorption isotherms, Eq. (4) allows part of the sites remain unoccupied. In ion exchange, however, an additional constraint is imposed and total charge of the mobile ions must exactly match the charge of the fixed groups at all conditions. When Eq. (4) is rewritten in terms of equivalent fractions  $y$  defined in Eq. (5), an explicit ion exchange isotherm shown in Eq. (6) is obtained. For univalent ions and with  $h_i = 1$ , this expression becomes identical with the mass action formulation conventionally used in ion exchange. For other cases, Eq. (6) retains the explicit form while the mass action formulation must be solved iteratively. Moreover, the thermodynamic consistency of the original NICA isotherm [21] is conserved.

$$y_i = \frac{|z_i|q_i}{|z_R|q_{max}} \quad (5)$$

$$\sum_{j=1}^N y_j = 1$$

$$q_i = \frac{|z_R|q_{max}h_i(K_i c_i)^{h_i}}{\sum_{j=1}^N |z_j|h_j(K_j c_j)^{h_j}} \quad (6)$$

### 2.2.2. Calculations

Several simplifying assumptions were made in order to reduce the calculation time needed in simulation of the very long loading steps. The simplifications can be summarized as follows.

- (1) Partial differential balances in axial and radial direction were approximated using the stirred tanks-in-series and LDF models.
- (2) External mass transfer resistance was not explicitly considered.
- (3) Solution phase was considered ideal.
- (4) Speciation equilibria were omitted.

The set of stiff ordinary differential equations (Eq. (1)) was solved using the backward differentiation formula. Initial and boundary conditions for a given column are given in Eq. (7).

$$\begin{aligned}
 t = 0 : c_i(x) &= c_i^0(x) \text{ or } c_i(k) = c_i^0(k) \\
 q_i(x) &= q_i^0(x) \text{ or } q_i(k) = q_i^0(k) \\
 t > 0 : v &= \frac{\sum_j \dot{V}_{in,j}}{\varepsilon_b A_b} \\
 c_i^{feed} &= \frac{\sum_j c_{i,j}^{in} \dot{V}_{in,j}}{\sum_j \dot{V}_{in,j}} \\
 c_i|_{k=1} &= c_i^{feed}
 \end{aligned} \quad (7)$$

Here  $c^0$  is the initial liquid-phase concentration in the resin bed and  $q^0$  is the corresponding value in the resin calculated from Eq. (6).  $\dot{V}_{in}$  is the volumetric flow rate of inlet stream and  $c^{in}$  is the concentration therein. Summation goes over all streams entering the column and  $c^{feed}$  is the resulting inlet concentration. Axial dispersion coefficient,  $D_{ax}$ , was estimated from the correlation of Chung and Wen [22], and Eq. (2) was used to calculate appropriate value for  $N$ .

The calculation procedure was as follows. After computing the initial condition for the resin beds, the system configuration was defined for the first cycle ( $0 < t \leq \tau$ ), where  $\tau$  is the cycle time. Input and outlet stream matrices for each column were indexed, and the feed flow rates and feed concentrations were calculated from Eq. (7). Each column was consecutively calculated and the outlet history of each column as well as the concentration profiles at  $t = \tau$  were stored. After the first cycle, the input and outlet stream matrices were reindexed in order to mimic shift of the inlet and outlet ports. Then the columns were calculated from  $t = \tau$  to  $t = 2\tau$  using the results from the first cycle as new initial and boundary conditions. This procedure was continued until the desired number of cycles was computed.

Parameters for the equilibrium and mass transfer model were estimated from the breakthrough curves by trial-and-error. This approach was selected because no independent equilibrium or kinetic data were available, and the experimental data covered only one feed composition per system. Goodness of fit was estimated using the average relative deviation defined in Eq. (8), where  $N_{dp}$  is number of data points.

$$\text{ARD} = \frac{1}{N_{dp}} \sum_{j=1}^{N_{dp}} \left| \frac{c_{out,exp} - c_{out,calc}}{c_{out,exp}} \right| \times 100\% \quad (8)$$

### 3. Results and discussion

#### 3.1. Correlation of the breakthrough data

In the first step, reasonable values were estimated for the model parameters using the experimental breakthrough curves shown in Figs. 1 and 2 for the HFO and SBA resins, respectively. The HFO resin was assumed to be initially in  $\text{HCO}_3^-$  form and the SBA resin in  $\text{Cl}^-$  form. Some parameters were fixed a priori (e.g. some  $h$  values in Eq. (6)) and others were found by trial and error. The values used in calculations are listed in Table 2.

It is obvious from Fig. 1 that the simplified model cannot fully explain breakthrough of As(V) in the HFO resin bed. Therefore, good correlation was attempted at low concentrations lying around the acceptable value of  $10 \mu\text{g/L}$ . In this way, the ARD value calculated from Eq. (8) values was 14%. When considering the shape of the As(V) breakthrough curve, several possibilities exist. Assuming that the shape is dictated solely by equilibrium conditions, an isotherm of the anti-Langmuir-type is suggested. Such behavior is typically found in cases where ion exclusion by Donnan potential is operative. In the present case, however, both the anion exchanger matrix and the functional HFO phase are positively charged and no exclusion effect for the arsenate anion should be present. It is therefore more plausible that low intra-particle diffusion rate together with external film diffusion resistance is responsible for the observed curve shape. When a simplified LDF model (Eq. (3)) is used, the internal and external contributions are treated similarly and lumped in the apparent value of  $D_s$ .

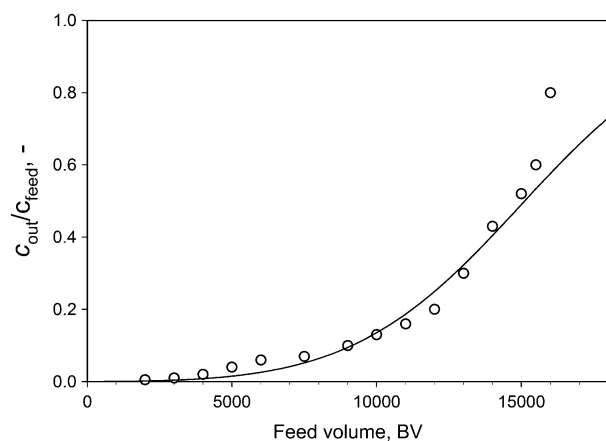


Fig. 1. Experimental and calculated breakthrough curves of As(V) for the HFO resin. Experimental data are taken from Cumbal and SenGupta [10]. Continuous line represents model calculations.

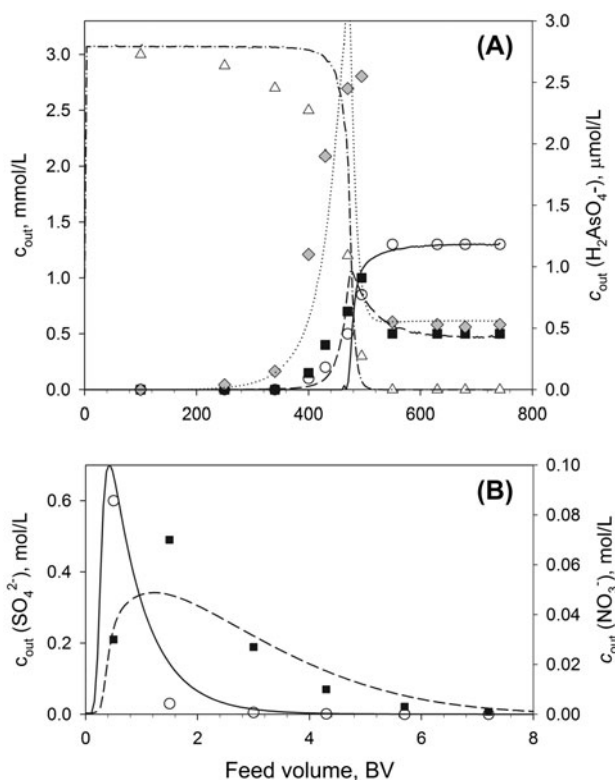


Fig. 2. Experimental and calculated breakthrough curves for  $H_2AsO_4^-$  (shaded diamonds, dotted line),  $SO_4^{2-}$  (open circles, solid line),  $NO_3^-$  (filled squares, dashed line) and  $Cl^-$  (open triangles, dash-dotted line) in the SBA resin. Experimental data are taken from Kim and Benjamin [14]. (A) Loading step and (B) regeneration step. Continuous lines are model calculations.

Table 2  
Model parameters used in calculations

Ion	$\log K$ ( $K$ in L/mol)	$h$ (-)	$D_s$ ( $10^{-12}$ m <sup>2</sup> /s)
HFO resin, $D_{ax} = 4 \times 10^{-7}$ m <sup>2</sup> /s			
$SO_4^{2-}$	0.00	0.50	1.0
$HCO_3^-$	-1.00	1.00	3.0
$Cl^-$	-1.00	1.00	3.0
$H_2AsO_4^-$	4.03	1.00	0.0080
SBA resin, $D_{ax} = 7 \times 10^{-7}$ m <sup>2</sup> /s			
$SO_4^{2-}$	-5.3	0.20	10
$NO_3^-$	0.25	1.0	30
$Cl^-$	0.0	1.0	30
$H_2AsO_4^-$	0.05	1.0	30

In fact, a very low value of  $8 \times 10^{-14}$  m<sup>2</sup>/s was obtained for  $D_s$  of the arsenate ion in the HFO resin. This is due to its high selectivity to the HFO sites. The selectivity order is  $H_2AsO_4^- \gg SO_4^{2-} > HCO_3^-$  and in a

simplified treatment of diffusion in the gel-type resin, the high  $K$  value in Eq. (6) is taken into account only at the outer resin surface and elsewhere it becomes included in the apparent diffusion coefficient. The apparent value estimated here is quite similar to the value  $D_s = 5.5 \times 10^{-15}$  m<sup>2</sup>/s reported by DeMarco et al. [4] for As(V) diffusion in hybrid material containing HFO particles in a gel-type cation exchanger. Because the HFO resin also has a swollen gel structure, it is understandable that the values are of same order of magnitude. In order to obtain physically more relevant values for  $D_s$ , a heterogeneous model should be considered with local equilibrium calculated at every radial position. This approach means, however, substantial increase in computational burden and the calculation times become unreasonable long.

Regeneration of the HFO bed involves desorption with 10% NaOH and reprotonation with CO<sub>2</sub>-sparged water [10]. As the focus in the present study is on the efficiency of resin use during loading, these steps were not modeled in detail. Instead, the loaded resin was directly equilibrated with a solution, which renders the resin back to the original protonated form with  $HCO_3^-$  as the counter-ion.

As shown in Fig. 2, the breakthrough data in the SBA bed can be correlated reasonably well with the proposed model and the parameters given in Table 2. The ARD values obtained for loading and regeneration steps were 39 and 30%, respectively. Despite the large average deviations, the result is surprisingly good considering that the selectivity coefficients are known to vary in wide limits at the conditions of loading and regeneration, respectively. For the present system, Kim and Benjamin [14] have found that the binary selectivity coefficient for the sulfate/nitrate pair increases more than 1.5 orders of magnitude when going from low to high ionic strength conditions. In the loading step, the resin is contacted with the feed water containing about 0.003 mol/L of ions. Much higher ionic strength of 3–4 mol/L is found in the regeneration step, where the loaded resin is contacted with 3 M NaCl. It is therefore impossible to describe both loading and regeneration steps with constant selectivity coefficients. However, when Eq. (6) is used to describe the competitive uptake of ions, it is possible to find a parameter combination that produces the dependence of selectivity coefficient on the solution conditions. Admittedly, the parameters carry very little physical significance because several factors causing deviations from ideal behavior are lumped together. In any case, the results are encouraging for correlative purposes because the whole loading regeneration cycle can be described with a single set of parameters.

As shown in Table 2, diffusion coefficients of all ions in the SBA resin are of the same order of magnitude because only moderate differences in selectivity are present. The selectivity decreases in the order  $\text{SO}_4^{2-} > \text{NO}_3^- > \text{H}_2\text{AsO}_4^- > \text{Cl}^-$ .

In summary, the experimental breakthrough data taken from literature [10,14] can be correlated satisfactorily with the models proposed in this study. The challenge in modeling the highly selective HFO resin lies in the extremely low effective diffusion rate of As(V) in the resin. For the SBA resin, on the other hand, the difficulty lies in describing the selectivity behavior through the whole loading/regeneration cycle and the ion exchange model derived in this study appears successful for this purpose.

### 3.2. Intensification of As(V) removal with highly selective hybrid ion exchanger

Fixed beds of arsenic selective sorbents are usually scaled to allow treatment of 10,000–50,000 bed volumes of contaminated water [10,13]. With a typical empty bed contact time of 2–4 min, operating times ranging from 30 to 140 d are obtained. Moreover, shape of the As(V) breakthrough curves shown in Fig. 1 and elsewhere [12,13] is unfavorable for efficient use of the sorbent; when the loading is stopped at outlet concentration of 10  $\mu\text{g/L}$ , the bed is far from exhausted with arsenic and large portion of the resin remains unused. It is also important to note that, only about 20 bed volumes of desorption/regeneration solution is needed. Consequently, the other bed in a 2-column system is unused most of the time.

More efficient utilization of the resin capacity can in principle be achieved with counter-current operation with multiple columns and/or use of short beds. Counter-current operation in 3 columns is depicted in Fig. 3 and it is actually identical with the lead–lag concept [15]. However, the latter is usually operated discontinuously, while the process in Fig. 3 is a continuous counter-current SMB system. Application of the SMB system in As(V) removal with highly selective HFO resin is original contribution of this study.

In Fig. 3, a separate desorption/regeneration zone is used in similarity to the system used by Virolainen et al. [23] for ion exchange purification of hydrometallurgical streams. During the first cycle, contaminated water is fed in column 2 and the purified water is withdrawn from column 3. These two columns essentially form the conventional lead–lag system. At the same time, column 1 is treated with desorbent (NaOH solution) and regenerant ( $\text{CO}_2$ -sparged water) to remove bound arsenic and restore the HFO phase back to active condition.

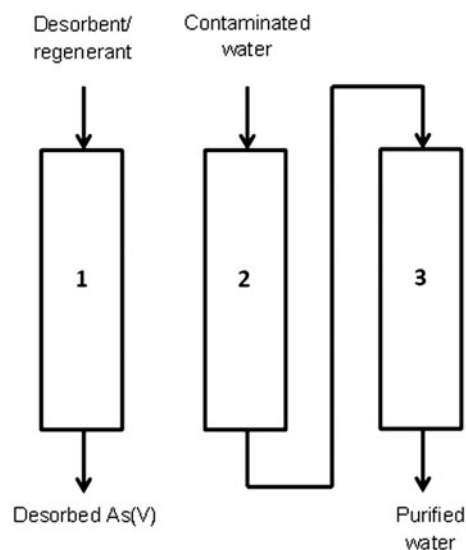


Fig. 3. Three-column SMB system for As(V) removal using the HFO resin.

After the first cycle, the inlet and outlet positions are shifted so that outlet of column 3 is connected to inlet of column 1, whereas desorbent and regenerant are directed to column 2. During the second cycle, contaminated water is fed in column 3 and purified water is taken from the regenerated column 1. Column 2, which is loaded as fully as possible, is desorbed and regenerated. This cyclic operation is continued and eventually a steady state is reached.

Operation of the loading zone of Fig. 3 was investigated by simulations using the equilibrium and kinetic model parameters listed in Table 2. First, the influence of bed length  $L$  was studied using values ranging from  $L_0$  to  $0.1L_0$ , where  $L_0$  is the bed length used in the experimental batch data of Fig. 1. Operating conditions for calculations are given in Table 3. Influence of the operating conditions was assessed in terms of productivity  $P$  defined by Eq. (9) and of arsenic loading in the resin. In Eq. (9),  $\dot{V}_{\text{in}}$  and  $V_{\text{resin}}$  are the inlet flow rate and total resin volume, respectively.

$$P = \frac{\dot{V}_{\text{in}}}{V_{\text{resin}}} \quad (9)$$

Product of the process is the purified water and target As(V) concentration was put at 5  $\mu\text{g/L}$ , which is half of the limiting value set by WHO. The SMB system was simulated until steady state was attained and the cycle time was adjusted in order to attain the target outlet arsenic concentration. Typically 40 cycles were

Table 3  
Operating conditions used in simulation of the 3-column system of Fig. 3

$L/L_0$	Feed flow rate (BV/h)	EBCT (min)	SLV (m/h)	Cycle time (h)
1	15.4	3.9	0.60	1,000
0.7	22.0	2.7	0.60	670
0.4	38.5	1.6	0.60	250
0.2	77.0	0.78	0.60	25
0.1	154	0.39	0.60	0.5

sufficient to establish the steady state and the behavior observed with  $L/L_0 = 0.1$  is depicted in Fig. 4.

The steady state results obtained with different relative bed heights are shown in Fig. 5.

Fig. 5 clearly demonstrates the strong effect of bed height on the productivity. This means that the same production rate and water quality can be achieved with a substantially smaller resin inventory in a shorter bed. With constant superficial linear velocity also the pressure drop decreases with decreasing bed height. At the same time, average As(V) loading in the “lead” column decreases markedly. If, for example, the bed height is 40% of the original value, the productivity doubles more from 5.1 to 12.8 h<sup>-1</sup>, but the resin loading decreases from 52.5 to 34.5 mmol/kg, mainly because of much shorter contact time (see Table 2). The cycle time is still very long in both cases (1,000 h for  $L/L_0 = 1$  and 250 h for  $L/L_0 = 0.4$ ) and the third column undergoing desorption/regeneration remains largely inactive. Increasing desorption/regeneration frequency is probably not a problem because the NaOH solution can be reused several times.

If very short beds ( $L/L_0 = 0.1$ ) are used, the cycle time of 0.5 h becomes closer to values normally used in SMB operations. Therefore, the loading and desorption/regeneration steps can be adjusted to avoid long

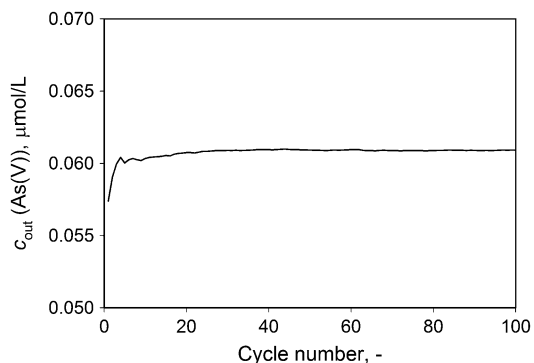


Fig. 4. Dependence of the As(V) concentration in the purified water on the cycle number in a 3-column SMB system.  $L/L_0 = 0.1$ .

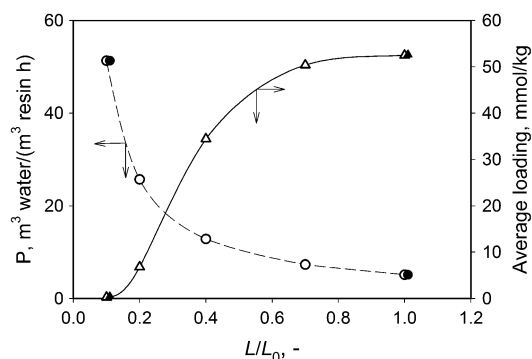


Fig. 5. Influence of bed height on the performance of a 3-column SMB system in As(V) removal. Circles and dashed line: productivity  $P$ ; triangles and solid line: average As(V) loading in the “lead” column. Open and filled symbols refer to SMB and batch operation, respectively.

off-stream times. With the shortest bed, productivity is 10 times as high as in the reference case ( $L/L_0 = 1$ ), but at the same time, resin loading with As(V) is very low. This means that the amount removed in each cycle is small and the desorption liquid must be recirculated in the system to compress desorbed As(V) in a reasonable volume before further treatment. It must be also noted that risk of arsenic leakage to the product water increases as the bed length decreases because of the mass transfer limitation in the As(V) uptake. As discussed earlier, the shape of the breakthrough curve in Fig. 1 most probably stems from the low effective diffusion rate of the arsenate ion. Consequently, very short contact times should be avoided.

The SMB results were also compared with those obtained with the batch system. It is important to understand that the situation in batch and continuous SMB ion exchange is different; in a batch system the As(V) concentration in the outlet increases gradually as shown in Fig. 1, while a constant average outlet concentration is produced in SMB. The loading time for the batch system with  $L/L_0 = 1$  was therefore adjusted so that the average outlet concentration was the same as in the case of SMB and a value of 1,650 h

was obtained. All other values were similar to those used for the SMB system. As shown in Fig. 5, practically the same results were obtained using simple batch operation. With batch operation and  $L/L_0 = 0.1$ , the loading time was 1.0 h and average As(V) loading was 0.45 mmol/kg, which is somewhat higher than found in the SMB system. It seems therefore that no additional advantage can be achieved in water purification by changing from the batch system to more complicated SMB system when the affinity of the impurities to be removed is as high as with the HFO resin.

In these calculations only bed height and operation mode (batch vs. counter-current SMB) were varied, while feed rate and column diameter were kept constant (constant SLV). More comprehensive optimization could maybe reveal more advantageous operating conditions, but the basic situation remains unchanged. First, productivity of the system can be increased substantially by optimizing the volume of the resin bed for a given feed rate. Secondly, the mass transfer limitations in As(V) uptake are critical in short bed operations. Finally, the calculations clearly indicate that simple batch operation is as effective as the more complicated counter-current SMB. These arguments probably apply to other analogous applications including removal of phosphate [24] and perchlorate [16] or capture of radionuclides from radioactive waste streams [25].

### 3.3. Simulation of As(V) removal with the SBA resin

The process configuration used in arsenic removal with the SBA resin is basically similar to that shown in Fig. 3 for the HFO resin. The mechanism of removal is, however, completely different as discussed in detail by Kim and Benjamin [14] and Chiavola et al. [9]. Selectivity of the arsenate anions in SBA resin is low and sulfate and nitrate anions present in the feed water are preferentially sorbed by the resin. The selectivity order is clearly seen in the breakthrough curve of Fig. 2 and the As(V) peak is located between the sulfate/nitrate fronts and the chloride front. During the first cycle of continuous SMB system, the arsenic peak is collected in column 3 and the “lead” column 2 becomes saturated with the feed solution and the resin contains mostly sulfate and nitrate. During the next cycle, the “lead” column is regenerated back to Cl form and the arsenic peak is again pushed to the “lag” column. The process is run continuously until arsenic starts to leak from the “lag” column to the product water. The system is therefore a counter-current SMB operated at non steady conditions. Exact cycle times have not been reported, but the data in Fig. 2

suggest a value of about 30 h, while the regeneration/washing step takes around 0.5 h [14]. The difference is much less than for the HFO resin but still the third column is mainly off-stream.

The original contribution of this study for the SBA resin case is twofold. First, the configuration is modified to render the system to a steady state SMB, where the removed As(V) is continuously withdrawn from the system. Secondly, more efficient use of the resin and higher productivity is attempted by decreasing the bed height. The SMB configuration used in simulations is depicted in Fig. 6; an extra column was added in order to allow As(V) withdrawal from column 3. The operating conditions used in simulations are listed in Table 4. Total outlet flow was kept constant and during the short period of concentrate withdrawal, the product water line was closed. Regeneration was again made separately (column 1 in Fig. 6) and as seen in Table 4, the regeneration time is always much shorter than the loading time. Relative length of the regeneration step is not much affected by  $L/L_0$  because the SBA bed to be regenerated is fully saturated with the feed irrespective of the value  $L/L_0$ .

As shown in Table 4, only a small volume of the As(V) concentrate is withdrawn from the system and therefore attainment of the steady state takes a very long time as compared with the HFO case shown in Fig. 4. Dependence of the outlet concentrations on the number of cycles is depicted in Fig. 7 for the case  $L/L_0 = 0.2$ . It should be emphasized, however, that the product (purified water) meets the specification right from the startup. In this case, the volume of the As(V) solution withdrawn during each cycle constitutes 1.8% of the total input of the contaminated water. The As

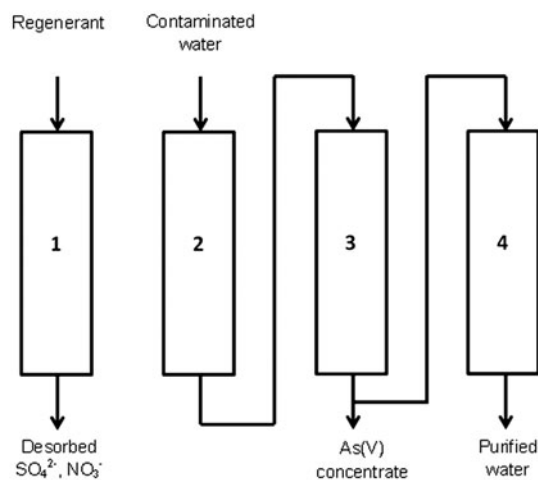


Fig. 6. Four-column SMB system for As(V) removal using the SBA resin.

Table 4  
Operating conditions used in simulation of the 4-column system of Fig. 6

$L/L_0$	Feed flow rate (BV/h)	EBCT (min)	SLV (m/h)	Cycle timing (min)				
				Total	Feed	Product	Concentrate	Regeneration
1	15.9	3.77	2.78	1,300	1,300	1,270	30	40
0.2	79.5	0.75	2.78	280	280	275	5	10

(V) concentration in the concentrate stream at steady state is more than 20 times the value found in the feed. There was also a low concentration of As(V) in the regeneration brine because the model parameters predict a slightly too high arsenic uptake in the “lead” column (column 2 in Fig. 6). The bound As(V) is then desorbed together with sulfate and nitrate ions.

In order to illustrate the conditions attained at steady state, the concentration profiles in the solution and resin phases are shown in Fig. 8. Accumulation of As(V) as a narrow band is clearly seen around the junction of columns 3 and 4. Because of the profile shape, arsenic concentration in the concentrate stream is very sensitive to the position of the band with respect to the outlet point. Therefore, the value shown in Fig. 7 for the As(V) concentrate is typical but even higher values can be obtained by careful adjustment of the cycle time and flow rates.

The simulation results indicate that steady state operation of the SBA resin system proposed in this study is possible. The advantage of this mode is that the accumulated As(V) can be continuously withdrawn from the system without intermittent regeneration of the “lag” column employed by Kim and Benjamin [14]. Because of the shape of the concentrated arsenic band,

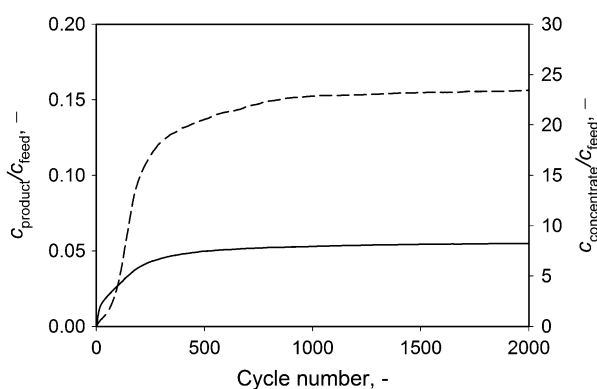


Fig. 7. Attainment of the steady state in continuous As(V) removal using the SBA resin.  $L/L_0 = 0.2$  and other operating conditions are given in Table 4. Relative concentrations in the product water and As(V) concentrate are given as solid and dashed lines, respectively.

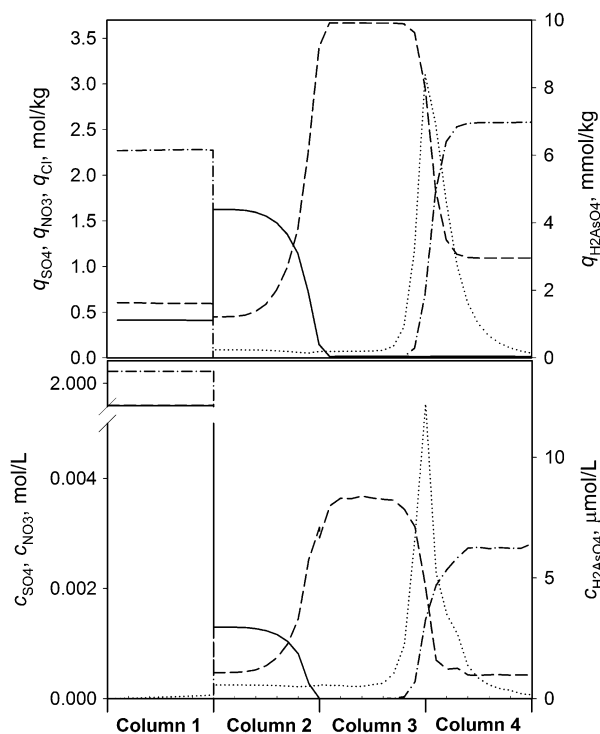


Fig. 8. Calculated steady state concentration profiles for  $\text{H}_2\text{AsO}_4^-$  (dotted line),  $\text{SO}_4^{2-}$  (solid line),  $\text{NO}_3^-$  (dashed line) and  $\text{Cl}^-$  (dash-dotted line) in the SBA resin.  $L/L_0 = 0.2$  and other operating conditions are given in Table 4. The column indices refer to Fig. 6.

control of the truly continuous system may, however, be difficult and risk of movement of the concentrated As(V) band toward the outlet of purified water exists.

The data shown in Figs. 7 and 8 were obtained with a shallow bed ( $L/L_0 = 0.2$ ) and with 95% removal of As(V). When compared with the values calculated using the original bed height ( $L/L_0 = 1.0$ , 93% removal of As(V)), the system productivity increased from 3.98 to 19.9  $\text{m}^3$  water/ $(\text{m}^3$  resin h).

#### 4. Conclusions

In this study, we have numerically simulated ion exchange of As(V) in two fundamentally different cases. The HFO resin containing HFO is highly

selective for As(V), while the SBA resin preferentially sorbs other anions ( $\text{SO}_4^{2-}$ ,  $\text{NO}_3^-$ , etc.) present in the feed water. We have shown the following.

- (1) Relatively simple models can be used to correlate the breakthrough data of As(V) in beds of both resins. Such models together with parameters adjusted against experimental data allow simulation and optimization of actual purification processes.
- (2) For the HFO resin, comparison between continuous SMB and batch operation shows that the latter is the best option and no further advantage is gained using more complicated process configurations.
- (3) Removal of As(V) with the SBA resin can be realized only in a SMB system and it is possible to use a steady state continuous process, where the concentrated As(V) solution is continuously withdrawn from the system.
- (4) In both systems, productivity can be substantially increased using shallow resin beds and short cycle times.

### Acknowledgements

Financial support from the Academy of Finland (project ID 252688) and Tekes, Finland (IX Hydro project in ELEMET programme) is gratefully acknowledged.

### List of symbols

$A_b$	—	cross-sectional area of the bed ( $\text{m}^2$ )
$c$	—	concentration (mol/L)
$d_s$	—	particle diameter (m)
$D_s$	—	diffusion coefficient ( $\text{m}^2/\text{s}$ )
$D_{\text{ax}}$	—	axial dispersion coefficient ( $\text{m}^2/\text{s}$ )
$h$	—	NICA parameter (–)
$K$	—	affinity constant (L/mol)
$L_b$	—	length of the bed (m)
$N$	—	number of mixing stages (–)
$p$	—	NICA parameter (–)
$\bar{q}$	—	volume-averaged concentration in resin (mol/kg)
$q_{\text{max}}$	—	maximum uptake capacity (mol/kg)
$t$	—	time (s)
$v$	—	interstitial flow velocity (m/s)
$\dot{V}$	—	volumetric flow rate (L/s)
$z$	—	ion charge (–)
$\varepsilon_b$	—	bed porosity (–)
$\rho_s$	—	solid content in the swollen resin (kg/L)

### Abbreviations

EBCT	—	empty bed contact time
HFO	—	hydrous ferric oxide
NICA	—	non-ideal competitive adsorption
SBA	—	strong base anion exchanger
SLV	—	superficial fluid velocity

### References

- [1] D. van Halem, S.A. Bakker, G.L. Amy, J.C. van Dijk, Arsenic in drinking water: A worldwide water quality concern for water supply companies, *Drink. Water Eng. Sci.* 2 (2009) 29–34.
- [2] C. Li, S. Kang, P. Chen, Q. Zhang, J. Mi, S. Gao, M. Sillanpää, Geothermal spring causes arsenic contamination in river waters of the southern Tibetan Plateau, China, *Environ. Earth Sci.* 71 (2014) 4143–4148.
- [3] E. Repo, M. Mäkinen, S. Rengaraj, G. Natarajan, A. Bhatnagar, M. Sillanpää, Lepidocrocite and its heat-treated forms as effective arsenic adsorbents in aqueous medium, *Chem. Eng. J.* 180 (2012) 159–169.
- [4] M.J. DeMarco, A.K. SenGupta, J.F. Greenleaf, Arsenic removal using a polymeric/inorganic hybrid sorbent, *Water Res.* 37 (2003) 164–176.
- [5] E.O. Kartinen, C.J. Martin, An overview of arsenic removal processes, *Desalination* 103 (1995) 79–88.
- [6] D. Mohan, C.U. Pittman, Arsenic removal from water/wastewater using adsorbents—A critical review, *J. Hazard. Mater.* 142 (2007) 1–53.
- [7] L. Dambies, Existing and prospective sorption technologies for the removal of arsenic in water, *Sep. Sci. Technol.* 39 (2004) 603–627.
- [8] J. Kim, M.M. Benjamin, P. Kwan, Y. Chang, A novel ion exchange process for As removal, *J. Am. Water Works Assoc.* 95 (2003) 77–85.
- [9] A. Chiavola, E. D'Amato, R. Baciocchi, Ion exchange treatment of groundwater contaminated by arsenic in the presence of sulphate. Breakthrough experiments and modeling, *Water Air Soil Pollut.* 223 (2012) 2373–2386.
- [10] L. Cumbal, A.K. SenGupta, Arsenic removal using polymer-supported hydrated iron(III) oxide nanoparticles: Role of Donnan membrane effect, *Environ. Sci. Technol.* 39 (2005) 6508–6515.
- [11] T. Tuutijärvi, E. Repo, R. Vahala, M. Sillanpää, G. Chen, Effect of competing anions on arsenate adsorption onto maghemite nanoparticles, *Chin. J. Chem. Eng.* 20 (2012) 505–514.
- [12] P. Sylvester, P. Westerhoff, T. Möller, M. Badruzzaman, O. Boyd, A hybrid sorbent utilizing nanoparticles of hydrous iron oxide for arsenic removal from drinking water, *Environ. Eng. Sci.* 24 (2007) 105–112.
- [13] S. Neumann, Arsenic removal with selective hybrid adsorbents, *Water Wastewater Asia* 1 (2011) 28–31.
- [14] J. Kim, M.M. Benjamin, Modeling a novel ion exchange process for arsenic and nitrate removal, *Water Res.* 38 (2004) 2053–2062.
- [15] Available from: <[http://50.244.15.10/techlib/Puro-lite/Arsenex-NP\\_FB\\_070804.pdf](http://50.244.15.10/techlib/Puro-lite/Arsenex-NP_FB_070804.pdf)>. Accessed Available from: 21.05.2014.

- [16] R.A. Tripp, D. Clifford, Selectivity considerations in modeling the treatment of perchlorate using ion-exchange processes, in: A. SenGupta, Y. Marcus (Eds.), *Ion Exchange and Solvent Extraction*, vol. 16, Marcel Dekker, New York, NY, 2004, pp. 267–338.
- [17] C. Sayer, R. Giudici, A comparison of different modeling approaches for the simulation of the transient and steady-state behavior of continuous emulsion polymerizations in pulsed tubular reactors, *Braz. J. Chem. Eng.* 19 (2002), doi: 10.1590/S0104-66322002000100007.
- [18] S. Melis, J. Markos, G. Cao, M. Morbidelli, Ion-exchange equilibria of amino acids on a strong acid resin, *Ind. Eng. Chem. Res.* 35 (1996) 1912–1920.
- [19] D.A. Dzombak, F.M.M. Morel, *Surface Complexation Modelling: Hydrous Ferric Oxide*, John Wiley and Sons, New York, NY, 1990.
- [20] B. Pakzadeh, J.R. Batista, Surface complexation modeling of the removal of arsenic from ion-exchange waste brines with ferric chloride, *J. Hazard. Mater.* 188 (2011) 399–407.
- [21] D.G. Kinniburgh, W.H. van Riemsdijk, L.K. Koopal, M. Borkovec, M.F. Benedetti, M.J. Avena, Ion binding to natural organic matter: Competition, heterogeneity, stoichiometry and thermodynamic consistency, *Colloids Surf. A* 151 (1999) 147–166.
- [22] S.F. Chung, C.Y. Wen, Longitudinal dispersion of liquid flowing through fixed and fluidized beds, *AIChE J.* 14 (1968) 857–866.
- [23] S. Virolainen, I. Suppala, T. Sainio, Continuous ion exchange for hydrometallurgy: Purification of Ag(I)–NaCl from divalent metals with aminomethylphosphonic resin using counter-current and cross-current operation, *Hydrometallurgy* 142 (2014) 84–93.
- [24] L.M. Blaney, S. Cinar, A.K. Sengupta, Hybrid anion exchanger for trace phosphate removal from water and wastewater, *Water Res.* 41 (2007) 1603–1613.
- [25] J. Lehto, L. Brodtkin, R. Harjula, E. Tusa, Separation of radioactive strontium from alkaline nuclear waste solutions with the highly effective ion exchanger SrTreat, *Nucl. Technol.* 127 (1999) 81–87.